The Astrophysical Journal, 779:52 (8pp), 2013 December 10 doi:10.1088/0004-637X/779/1/52

KECK SPECTROSCOPY OF GRAVITATIONALLY LENSED $z \simeq 4$ GALAXIES: IMPROVED CONSTRAINTS ON THE ESCAPE FRACTION OF IONIZING PHOTONS

Tucker A. Jones[1], Richard S. Ellis[2], Matthew A. Schenker[2], and Daniel P. Stark[3,4]
[1] Department of Physics, University of California, Santa Barbara, CA 93106, USA
[2] Department of Astrophysics, California Institute of Technology, MS 249-17, Pasadena, CA 91125, USA
[3] Department of Astronomy and Steward Observatory, University of Arizona, Tucson, AZ 85721, USA
Received 2013 April 25; accepted 2013 September 20; published 2013 November 25

ABSTRACT

The fraction of ionizing photons that escape from young star-forming galaxies is one of the largest uncertainties in determining the role of galaxies in cosmic reionization. Yet traditional techniques for measuring this fraction are inapplicable at the redshifts of interest due to foreground screening by the Lyα forest. In an earlier study, we demonstrated a reduction in the equivalent width of low-ionization absorption lines in composite spectra of Lyman break galaxies at $z \simeq 4$ compared to similar measures at $z \simeq 3$. This might imply a lower covering fraction of neutral gas and hence an increase with redshift in the escape fraction of ionizing photons. However, our spectral resolution was inadequate to differentiate between several alternative explanations, including changes with redshift in the outflow kinematics. Here we present higher quality spectra of three gravitationally lensed Lyman break galaxies at $z \simeq 4$ with a spectral resolution sufficient to break this degeneracy of interpretation. We present a method for deriving the covering fraction of low-ionization gas as a function of outflow velocity and compare the results with similar quality data taken for galaxies at lower redshift. We find an interesting but tentative trend of lower covering fractions of low-ionization gas for galaxies with strong Lyα emission. In combination with the demographic trends of Lyα emission with redshift from our earlier work, our results provide new evidence for a reduction in the average H I covering fraction, and hence an increase in the escape fraction of ionizing radiation from Lyman break galaxies, with redshift.

Key words: dark ages, reionization, first stars – galaxies: evolution – galaxies: formation – galaxies: ISM

Online-only material: color figures

1. INTRODUCTION

Star-forming galaxies are the leading candidate for the source of ultraviolet photons required to reionize the universe. Several lines of evidence indicate that reionization was underway by $z = 11$ and ended a few hundred Myr later at $z \simeq 6$–7 (e.g., Schenker et al. 2012; Mortlock et al. 2011; Hinshaw et al. 2013). Deep near-IR imaging with the *Hubble Space Telescope* (*HST*) has provided good constraints on the UV luminosity density of star-forming galaxies during the reionization epoch (e.g., Ellis et al. 2013; Oesch et al. 2013) that indicate that the ongoing star formation is likely capable of producing the required ionizing flux. However, it is unclear whether this radiation is able to escape from galaxies and actually ionize the intergalactic medium (IGM). Based on estimates of the total UV luminosity density and IGM clumping factor, the required escape fraction $f_{\rm esc}$ of hydrogen-ionizing photons is $\gtrsim$0.2 (e.g., Robertson et al. 2013). The precise value of $f_{\rm esc}$ is a key uncertainty in determining the role of galaxies in reionization.

Direct measurements of $f_{\rm esc}$ during the reionization epoch are essentially impossible, not only because of the faint apparent luminosity, but also because foreground IGM attenuates the ionizing flux to undetectable levels even at $z \gtrsim 4$. Inoue & Iwata (2008) calculate that only ∼20% of sources at $z = 4$ should have sight lines through the IGM for which escaping ionizing flux could plausibly be detected, and this number drops rapidly at higher redshift. Several studies based on direct imaging and composite spectra of galaxies at lower redshift have established a modest average $f_{\rm esc} \simeq 0.05$ for $\sim L^*$ Lyman break galaxies (LBGs) at $z = 3$ (e.g., Iwata et al. 2009; Bogosavljević 2010; Boutsia et al. 2011; Nestor et al. 2013). Studies at lower redshifts have found smaller escape fractions: Siana et al. (2010) found an upper limit $f_{\rm esc} < 0.02$ in UV-bright starburst galaxies at $z \sim 1.3$, and Leitet et al. (2013) have detected $f_{\rm esc} \simeq 0.015$ in stacked spectra of star-forming galaxies at $z = 0$. Although based on limited samples, these results suggest an increasing escape fraction at higher redshifts. Furthermore, $f_{\rm esc}$ must have been higher at earlier times if star-forming galaxies dominated reionization. Results from cosmological simulations show mixed trends with redshift but generally predict higher $f_{\rm esc}$ in low-mass galaxies (e.g., Razoumov & Sommer-Larsen 2010; Yajima et al. 2011; Paardekooper et al. 2013), in agreement with the available observations (Nestor et al. 2013) and predictions for "runaway" stars (Conroy & Kratter 2012).

This paper is concerned with improving the constraints on $f_{\rm esc}$ at higher redshifts for which direct measurements are not practical. Our methodology is as follows: $f_{\rm esc}$ is set by the areal covering fraction of hot stars by H I such that $f_{\rm esc} = 1 - f_c$, and f_c can be inferred from intermediate dispersion spectroscopy of interstellar UV absorption lines. This technique has also been employed at lower redshifts to examine the physical conditions that may give rise to escaping ionizing flux, and in particular Heckman et al. (2011) found low covering fractions in galaxies with independent evidence of high escape fractions based on Balmer recombination lines. The difficulty, of course, is that LBGs at redshift $z > 3$ are very faint, so securing suitably high quality absorption line spectra of individual examples is a very challenging proposition. In an earlier paper (Jones et al. 2012), we therefore analyzed the average properties of LBGs at $z \simeq 4$–5 derived from composite spectra in a manner similar to that pioneered at $z \simeq 3$ by Shapley et al. (2003).

A particular motivation for the present study was the discovery of a marked reduction with increasing redshift in the equivalent width of low-ionization absorption lines at fixed UV

[4] Hubble Fellow.

Table 1
Gravitationally Lensed Sources

ID	R.A.	Decl.	z	m_{AB}	M_{UV}[a]	t_{exp} (hr)	References
Abell 2390_H3a	21:53:34	+17:42:03	4.043 ± 0.002	$I = 22.4$[b]	-21.3 ± 0.3	10.8	Frye & Broadhurst (1998); Pelló et al. (1999)
Abell 2390_H5b	21:53:35	+17:41:33	4.0448 ± 0.0003	$I = 22.8$[b]	-21.0 ± 0.3	10.8	Pelló et al. (1999)
1621+0607	16:21:33	+06:07:05	4.1278 ± 0.0004	$I = 22.6$[c]	-21.0[d]	5.7	Bayliss et al. (2011)
cB58	15:14:22	+36:36:25	2.73	$r = 20.6$	-21.1		Pettini et al. (2002)
Cosmic Eye	21:35:13	−01:01:43	3.07	$r = 20.3$	-21.8		Quider et al. (2010)
Horseshoe	11:48:33	+19:29:59	2.38	$g = 20.1$	-21.5		Quider et al. (2009)
8 o'clock arc	00:22:41	+14:31:10	2.73	$r = 19.2$	$-23.4^{+0.9}_{-0.4}$		Dessauges-Zavadsky et al. (2010)
Q0000-D6[e]	00:03:24	−26:02:49	2.96	$R = 22.9$	-22.6		Steidel et al. (2010); Giallongo et al. (2002)

Notes.
[a] Unlensed absolute magnitudes at effective wavelength ∼1500 Å depending on filter and redshift.
[b] *HST*/WFPC2 F814W magnitude from Sand et al. (2005).
[c] Derived from the spectrum at the mean wavelength of *HST*/WFPC2 F814W, $\lambda_{mean} = 8369.5$ Å.
[d] For a magnification factor $\mu = 10$.
[e] This source is not gravitationally lensed.

luminosity, suggestive of changes in either the kinematic profile or the covering fraction of neutral gas (Jones et al. 2012). Additionally, spectra of individual galaxies show a trend of increasing Lyα emission equivalent width with redshift, which we argued could reflect evolution in the H I covering fraction (Stark et al. 2010), especially given the strong correlation of Lyα and low-ionization absorption lines (Shapley et al. 2003; Jones et al. 2012). We note that galaxies with stronger Lyα emission and weaker low-ionization absorption also tend to have bluer UV slopes indicative of lower dust extinction, which Shapley et al. (2003) argued is likely caused by dust entrained in the low-ionization gas. A lower covering fraction of this material naturally results in both weaker absorption and less dust extinction. Therefore, variations in the dust content of LBGs (e.g., Stark et al. 2010) may also signify evolution in the H I covering fraction with redshift. A lower covering fraction for the neutral gas within typical LBGs would be particularly important as it could imply a higher escape fraction of ionizing photons. The composite spectra discussed by Jones et al. (2012) did not have adequate resolution to distinguish the effects of reduced covering fraction and kinematics, and so the present paper takes this investigation one step further by attempting to resolve this important ambiguity. Here we present higher resolution spectra of three gravitationally lensed $z \simeq 4$ LBGs. Although their unlensed luminosities are typical of the constituent galaxies comprising the Jones et al. (2012) composite, their individual lensed magnitudes are much brighter, enabling comparable signal-to-noise ratio (S/N) to the stack of LBGs discussed in our earlier paper.

Throughout the paper, we adopt a flat ΛCDM cosmology with $\Omega_\Lambda = 0.7$, $\Omega_M = 0.3$, and $H_0 = 70$ km s^{-1} Mpc^{-1}. All magnitudes are in the AB system (Oke 1974).

2. GRAVITATIONALLY LENSED $z \simeq 4$ GALAXIES

The spectra composing the composite published by Jones et al. (2012) were taken with the 600 line mm^{-1} DEIMOS grating with a resolution of ≃3.5 Å, although uncertain systemic redshifts led to reduced resolution of the composite spectrum (corresponding to a velocity resolution of ∼450 km s^{-1} FWHM). The composite comprised galaxies with $z'_{AB} = 24$–26 with 90% completeness to $z'_{AB} = 25$ at $z \simeq 4$. The stacked spectrum reveals multiple low-ionization lines such as Si II λ1260, O I λ1302 + Si II λ1304, and C II λ1334 in the region where the S/N is optimal. As discussed by Jones et al. (2012), these lines are normally saturated so the line depth at a given velocity provides a measure of the areal covering fraction f_c of O and B stars by neutral H I gas along the line of sight.

Typical LBGs are too faint for detailed line profile studies even at $z = 2$, but strong gravitational lensing can boost the brightness of representative examples, making such studies of individual sources a practical proposition. Studies of several lensed $z \simeq 2$–3 LBGs have found that absorption velocities of low-ionization metal transitions range from ∼−1000 to +500 km s^{-1} with typical line centroids $v \sim -200$ km s^{-1} (Pettini et al. 2002; Quider et al. 2009, 2010; Dessauges-Zavadsky et al. 2010). The mean low-ionization absorption velocity in the Jones et al. (2012) composite is similar, $v_{LIS} = -190$ km s^{-1}.

In a similar fashion, for the present analysis we have located three gravitationally lensed LBGs at $z \simeq 4$. Two are independent sources lensed by the well-studied cluster Abell 2390, and the third was located in the cluster J1621+0607 in the Sloan Digital Sky Survey. A2390_H3 and H5 represent two distinct highly elongated pairs of lensed images that were spectroscopically confirmed to be at different redshifts by, respectively, Frye & Broadhurst (1998) and Pelló et al. (1999). The tangential arc system in J1621+0607 was spectroscopically confirmed by Bayliss et al. (2011). The gravitational magnification factor is ≃10 in each case (Pelló et al. 1999). We summarize the key properties in Table 1. The redshifts and absolute UV luminosities are representative of sources studied by Jones et al. (2012). In addition, for comparison purposes, we include an analysis of high-quality spectra for three further lensed $z = 2$–3 sources (courtesy of M. Pettini) in Table 1. These include the "Horseshoe" ($z = 2.38$; Quider et al. 2010), cB58 ($z = 2.73$; Pettini et al. 2002), and the "Cosmic Eye" ($z = 3.07$; Quider et al. 2009). We note that the unlensed luminosities of these three sources are typical of those used in the composite of Shapley et al. (2003) ($M_{UV} \simeq -21.5$ to -20.5). The other $z \sim 3$ comparison sources in Table 1, namely, the "8 o'clock arc" and Q0000-D6, are considerably brighter.

High-resolution *HST* images of each spectroscopic target are shown in Figure 1 with DEIMOS slit positions overlaid. Slits were oriented to encompass the entire galaxies. Spectra were taken with the 1200 line mm^{-1} DEIMOS grating during two runs in 2011 October and 2012 June. This provides a resolution of ≃1.7 Å corresponding to a velocity resolution of ≃70 km s^{-1}, considerably better than for the composite discussed by Jones

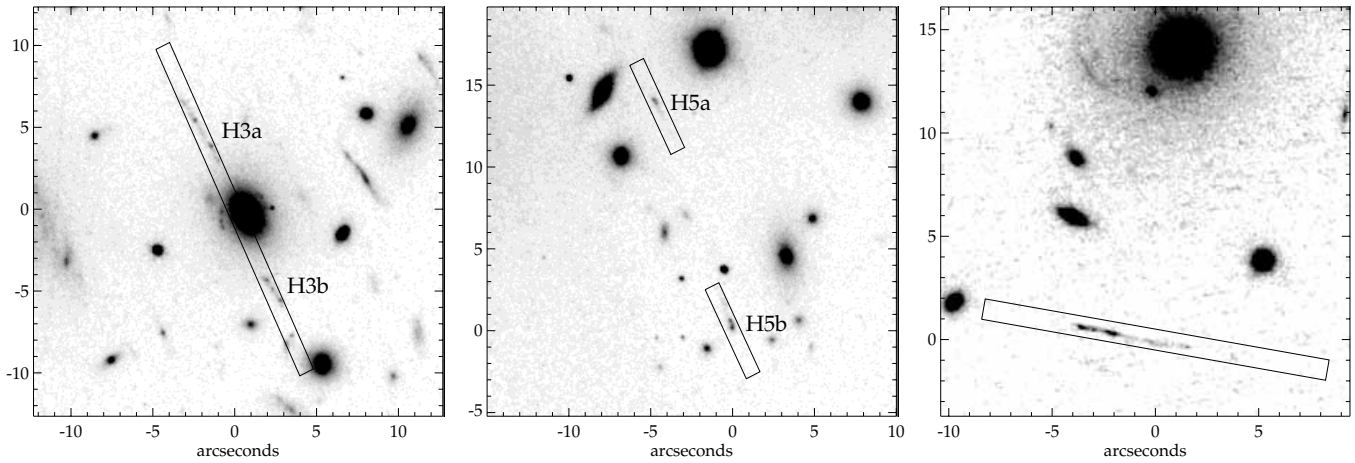

Figure 1. *HST* imaging of (left to right) A2390_H3, A2390_H5, and J1621 with DEIMOS slit positions overlaid. North is up and east is to the left. The instrument/filter is ACS/F814W for the A2390 arc images and WFC3/F775W for J1621, with central wavelengths similar to the DEIMOS spectra. In all cases the slit is oriented to include the entire source.

et al. (2012). Spectra of each galaxy covered the wavelengths corresponding to at least 1175−1675 Å in the rest frame. The lensed sources in Abell 2390 were observed simultaneously with a multi-slit mask that sampled two images of each source (Figure 1). Seeing varied between 0.″4 and 1.″4 FWHM during the observations, and the bulk of the data used have seeing in the range 0.″7–0.″9. Some exposures (∼10%) were affected by cirrus and are not included in the final addition. Total observing times for the final spectra are given in Table 1.

The DEIMOS spectra were reduced and calibrated using the Spec2D pipeline following the techniques discussed in detail by Stark et al. (2010). In the case of A2390_H3, care was taken to ensure that the extracted spectrum was not contaminated by light from a nearby cluster member. Data from the 2011 October and 2012 June runs were reduced separately, and the resulting one-dimensional spectra were combined with an inverse-variance weighted mean. Spectra of J1621 are affected by poor sky subtraction residuals, while the Abell 2390 arc spectra are of excellent quality. Spectra of different images of the Abell 2390 arcs were scaled to the same flux level before combining to a common wavelength scale with 0.7 Å pixels, roughly Nyquist sampled. The final spectra, shown in Figure 2, reach an average continuum S/N per 70 km s^{-1} resolution element of 5 for J1621, 9 for A2390_H3, and 10 for A2390_H5 over the rest-frame wavelength range 1250–1650 Å. This is comparable to that in the composite spectrum in Jones et al. (2012), which has S/N equivalent to ∼10 at the improved resolution of 70 km s^{-1} of our new data.

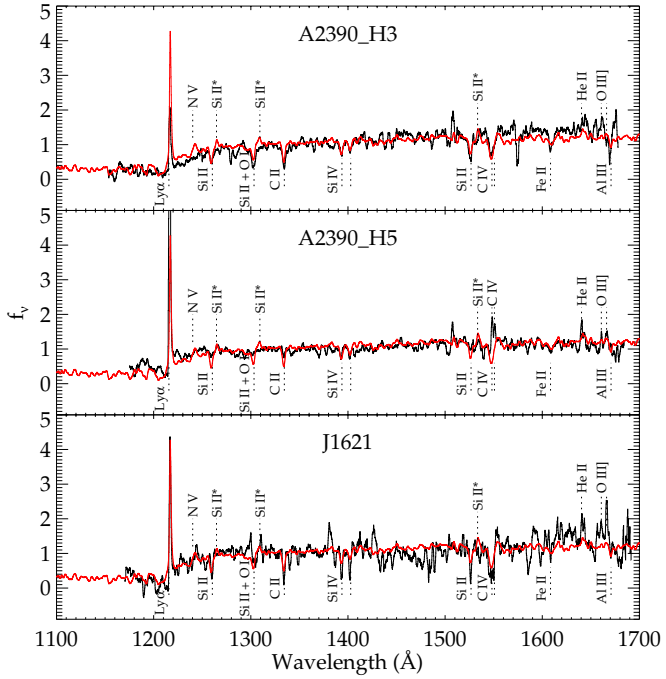

Figure 2. Keck DEIMOS spectra of (top to bottom) A2390_H3, A2390_H5, and J1621. In each panel the black spectrum represents the lensed galaxy and the composite spectrum of 81 LBGs from the analysis of Jones et al. (2012) is shown in red. All spectra are plotted in the rest frame with flux normalized such that median $f_\nu = 1$ in the range 1250–1500 Å. Prominent spectral features are labeled.

(A color version of this figure is available in the online journal.)

3. ANALYSIS

3.1. Systemic Redshift

Accurate systemic redshifts are required in order to examine the kinematics of gas seen in absorption, and the techniques for estimating these are discussed in detail in Jones et al. (2012). This is straightforward when nebular emission lines are visible, such as is the case in both J1621+0607 (O III] λλ1661, 1666) and A2390_H5 (O III] λλ1661, 1666, He II λ1640, C IV λλ1548, 1551). The strong emission from highly ionized species such as He II and C IV seen in A2390_H5 is uncommon but has been observed in some high-redshift starburst galaxies and signifies an extremely young, metal-poor, and hot stellar population (e.g., Fosbury et al. 2003; Erb et al. 2010). Alternatively, they may signify the presence of an active galactic nucleus, but the narrow line widths (50–185 km s^{-1} FWHM, corrected for instrumental resolution) suggest an origin in star-forming H II regions. We note that apparent emission near the wavelength of N v in J1621 is a sky line residual and is not a significant feature.

No appropriate features are detected in the spectrum of A2390_H3, and so we estimate the systemic redshift from low-ionization absorption lines using the method of Jones et al. (2012). This gives $z = 4.043 \pm 0.002 = z_{\rm IS} + 190$ km s^{-1}, with uncertainty dominated by an rms difference ∼125 km s^{-1} between redshifts derived from absorption lines and that

obtained from nebular emission (Steidel et al. 2010). The adopted systemic arc redshifts are listed in Table 1.

3.2. Low-ionization Covering Fraction

Ideally we would measure the covering fraction of neutral hydrogen directly from spatially resolved H I absorption. However, the only available transition (Lyα) is dominated by strong emission with net equivalent width $W_{\mathrm{Ly}\alpha} = 20$–$100$ Å when integrated within 100 kpc, and the observed line profile is complicated by resonant scattering in the extended circumgalactic medium (CGM; Steidel et al. 2011). These effects are apparent from the Lyα line profiles, which show redshifted emission as well as strong absorption arising from both the CGM and Lyα forest (Figure 2). We therefore estimate the covering fraction of neutral hydrogen from absorption lines of heavier low-ionization species that arise in H I gas, i.e., those with ionization potentials less than 1 Rydberg.

The covering fraction of any ion is related to its absorption line optical depth τ and residual intensity I via

$$\frac{I}{I_0} = 1 - f_c(1 - e^{-\tau}), \quad (1)$$

where I_0 is the continuum level. Optical depth is in turn related to column density as

$$\tau = f\lambda \frac{\pi e^2}{m_e c} N = f\lambda \frac{N}{3.768 \times 10^{14}}, \quad (2)$$

where f is the ion oscillator strength, λ is the transition wavelength expressed in Å, and N is the ion column density in cm^{-2} (km s^{-1})$^{-1}$. Combining Equations (1) and (2) yields an expression for f_c as a function of I and N. In cases where two or more transitions are measured for the same ion, from the same ground state, with different values of $f\lambda$, it is possible to solve these equations for N and f_c. In the following analysis, we will treat all variables as functions of velocity, i.e., $f_c(v)$.

For the low-ionization species of interest, our spectra cover three such transitions of Si II at 1260, 1304, and 1526 Å, which we use to measure the covering fraction as a function of velocity $f_c(v)$, for each galaxy. Si II λ1304 is only used in the velocity range $v \gtrsim -200$ km s^{-1} where it is not contaminated by O I λ1302. We determine the continuum level I_0 from a running median of the spectrum in regions with no strong interstellar or stellar features, and we use this to normalize each spectrum. Based on the S/N and residual sky levels, we estimate the uncertainty in I_0 to be $\lesssim$5%. We then resample each Si II transition to a common velocity scale and find the values of N and f_c that minimize the least-square residual $\chi^2 = \sum (I_{\mathrm{obs}} - I_{N,f_c})^2/\sigma^2_{\mathrm{obs}}$ in each velocity bin. While resampling leads to correlated errors, the range of correlation is less than one spectral resolution element. We additionally find the range of N and f_c for which χ^2 is within 1 of the minimum value and adopt this as the uncertainty. We note that this confidence interval corresponds to the formal 1σ uncertainty only in the velocity range where all three transitions are used.

The best-fit f_c and uncertainty calculated for each arc are shown as a function of velocity in Figure 3. Since Si II is the dominant ion of silicon in H I gas, this is approximately equal to the covering fraction of H I (provided that it is enriched with Si), which impedes the escape of ionizing radiation. Figure 4 shows the individual Si II line profiles used to calculate f_c. The consistency of absorption lines with different optical depth suggests that in general these transitions are optically thick.

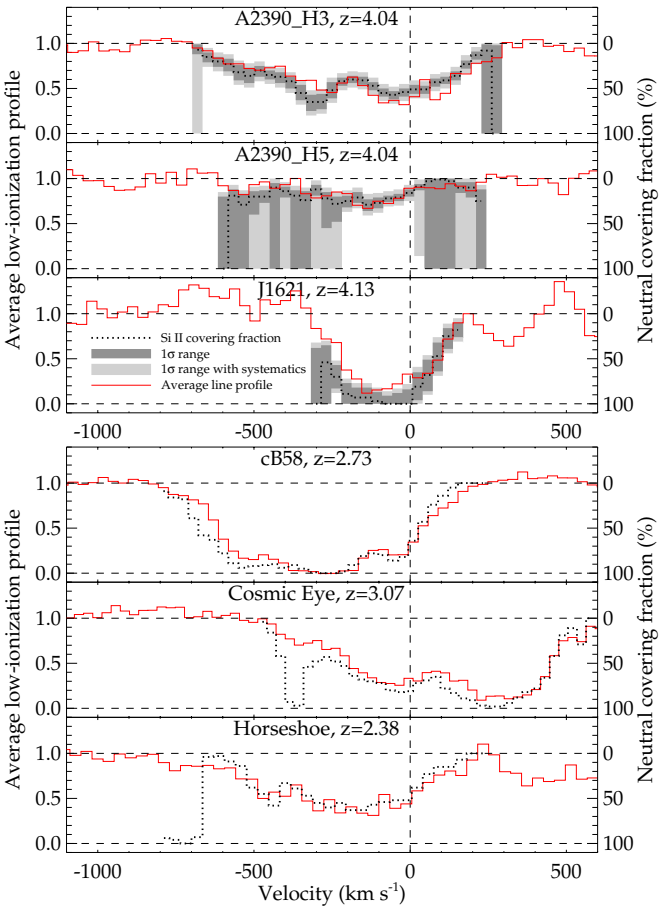

Figure 3. Mean low-ionization absorption line profile and its associated neutral gas covering fraction derived using the methods discussed in Section 3. Si II covering fraction of the $z \simeq 4''$ is measured from smoothed spectra with FWHM resolution $\simeq$110 km s^{-1}, while average line profiles are from unsmoothed data (FWHM $\simeq$ 70 km s^{-1}). There is no significant difference in results derived from the smoothed and unsmoothed spectra. Velocities are relative to adopted systemic redshifts (Section 3.1), derived from absorption line centroids for A2390_H3 and nebular emission in the other two cases. Equivalent measurements from ESI spectra of $z = 2''$–$3''$ are shown for comparison. Details of these ESI spectra can be found in Pettini et al. (2002) and Quider et al. (2009, 2010). For the $z \simeq 4''$, dark gray shading shows the uncertainty range based on random noise in the data, while lighter gray includes the effect of a 5% systematic error in the continuum level.

(A color version of this figure is available in the online journal.)

3.3. Average Low-ionization Absorption Profile

A simple and complementary alternative to the method outlined in Section 3.2 is to estimate the covering fraction from saturated transitions. In cases where $\tau \gg 1$, Equation (1) simplifies to

$$f_c = 1 - I/I_0. \quad (3)$$

Several of the strongest absorption lines covered by our spectra are typically saturated, including Si II λ1260, O I λ1302, Si II λ1304, C II λ1334, and Si II λ1526, which are all tracers of H I gas. In order to minimize the statistical uncertainty, we calculate the average intensity of these transitions as a function of velocity using an inverse-variance weighted mean, taking care not to use the wavelength region where O I λ1302 and Si II λ1304 are blended (roughly $-300 \lesssim v \lesssim -200$ km s^{-1} depending on the kinematics of each source). These profiles are shown in Figure 3 together with the covering fraction measured from Si II. We note that the covering fraction derived from Equation (3) is a strict lower limit.

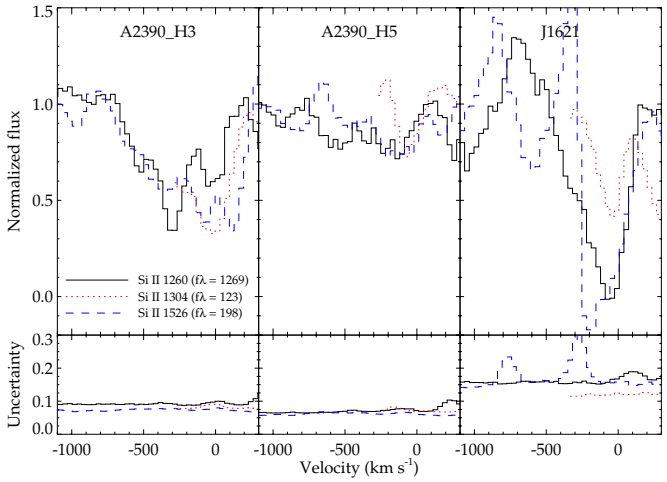

Figure 4. Individual Si II absorption line profiles and 1σ uncertainties, illustrating the technique introduced in Section 3.2. The various line profiles are generally consistent despite having optical depths $\tau \propto f\lambda$ that differ by a factor of $\sim$10, thereby indicating that the gas is optically thick. Residual flux in these transitions therefore indicates a partial covering fraction $f_{\rm cov}$ of Si II, which we calculate by solving Equations (1) and (2) and show in Figure 3. In cases of weak absorption (comparable to the noise level), we cannot distinguish between (a) optically thick gas with low covering fraction and (b) optically thin gas with high covering fraction. This is most apparent for A2390_H5, which shows a wide range of permissible $f_{\rm cov}$ in Figure 3.

(A color version of this figure is available in the online journal.)

4. RESULTS

This work was motivated in large part by the need to disentangle kinematics and covering fractions of absorbing gas. In particular, we seek to explain the extent to which decreased absorption line equivalent widths measured from composite spectra in our earlier work (Jones et al. 2012) result from changes in gas kinematics compared to covering fractions, as well as the implications of this result for the escape of ionizing radiation. We are limited in examining the redshift evolution of these properties by the small number of sources with suitable spectra, and we caution that this sample is not necessarily representative of the LBG population at these redshifts. Nonetheless, we can examine general trends within the existing data from this work and others in the literature (Pettini et al. 2002; Quider et al. 2009, 2010; Dessauges-Zavadsky et al. 2010). Following the methods in Section 3, we show the average absorption profiles and Si II covering fractions (derived from unblended transitions at 1260, 1526, and 1808 Å) of well-studied $z = 2$–3 galaxies for comparison in Figure 3. To quantify trends in the absorption line profiles, the velocity extent and maximum absorption depth for each galaxy are shown as a function of redshift in Figure 5.

In the case of Abell 2390, we take the most conservative approach, noting that the interpretation of the absorbing gas is complicated by the physical proximity and similar redshift of the two arcs. Their projected separation is $\sim$70 kpc (Pelló et al. 1999), and it is unclear which source lies in the foreground. At lower redshifts, Steidel et al. (2010) have shown that low-ionization absorption seen in a background source at $b = 70$ kpc has a detectable average equivalent width $\sim$0.4 Å for the transitions of interest. Since we lack specific information about the three-dimensional geometry, the following analysis does not include any contribution from this effect. If anything, our results will overestimate the true covering fraction and therefore yield a more conservative constraint on the escape fraction.

4.1. Kinematics

The kinematics of foreground low-ionization gas are revealed in the absorption line profiles shown in Figure 3. In all cases we see significant blueshifted absorption indicating outflows, as expected given the high star formation surface densities (Heckman 2002). The maximum outflow velocity at which absorption is detected is -700 km s^{-1} in A2390_H3, with an uncertainty of $\sim$125 km s^{-1} since we do not directly measure the systemic redshift. A2390_H5 reveals weak absorption extending to -600 km s^{-1}, seen also in higher ionization Si IV and C IV lines, although it is only marginally detected at <-300 km s^{-1}. The maximum outflow velocity in J1621 is -300 km s^{-1}.

The outflowing low-ionization gas attains a somewhat lower ($30\% \pm 20\%$ on average) maximum velocity in the $z = 4$ sample compared to $z \simeq 3$. This difference is not due to lower quality data as remains evident in Figure 3 if we consider alternative measures such as the FWHM or an absorption threshold at 25% of the continuum flux. However, the difference is not statistically significant, and all galaxies except J1621 have similar maximum velocities ranging from 600 to 800 km s^{-1}. Likewise, the extent of redshifted absorption is approximately +200 km s^{-1} for all sources, with the notable exception of the Cosmic Eye as discussed in detail by Quider et al. (2010); this indicates relatively little difference in line broadening from rotation or other internal kinematic structure. Therefore, in this limited sample, the low-ionization gas kinematics have little variation.

4.2. Covering Fraction

The covering fraction of each galaxy as a function of gas velocity is estimated from the methods described in Section 3 and shown in Figure 3. Both methods are generally in good agreement, indicating that Equation (3) is a valid approximation. Si II covering fractions derived for the Cosmic Eye are systematically higher than indicated by the average absorption profile; this is largely an artifact caused by additional absorption at the wavelength of Si II λ1260 from intervening gas at $z = 2.66$ (Quider et al. 2010). It is also apparent from Figure 3 that the Si II covering fraction is poorly constrained in regions of weak absorption due to the marginal significance of individual absorption lines. This is most problematic in the high-velocity wings. The strong anticorrelation between absorption line strength and covering fraction, as well as results at lower redshift (Martin & Bouché 2009), suggests that the most likely solution for such ambiguous cases is a low covering fraction of optically thick gas. We therefore opt to compare galaxies on the basis of their average absorption line profile as this quantity is simpler to define and less susceptible to the uncertainties described above. Nonetheless, the Si II results are an important verification that the average profile accurately traces f_c.

We can now compare the covering fractions measured at $z = 4$ with sources at lower redshift. Figure 5 shows the maximum absorption depth for each galaxy as a function of redshift. The $z = 4$ galaxies have maximum absorption depths corresponding to $f_c = 0.3$–0.9, in each case occurring at $v \sim -100$ km s^{-1}. There is a large scatter in Figure 5 with $\sigma(f_{c,\rm max}) = 0.26$ and no strong redshift dependence. Galaxies at $z = 4$ have covering fractions that are lower on average by $26\% \pm 25\%$ or $\Delta f_{c,\rm max} = 0.16$ compared to $z = 2$–3. The two populations are therefore consistent within the sample variance; a larger sample would be required to determine whether there is any evolutionary trend.

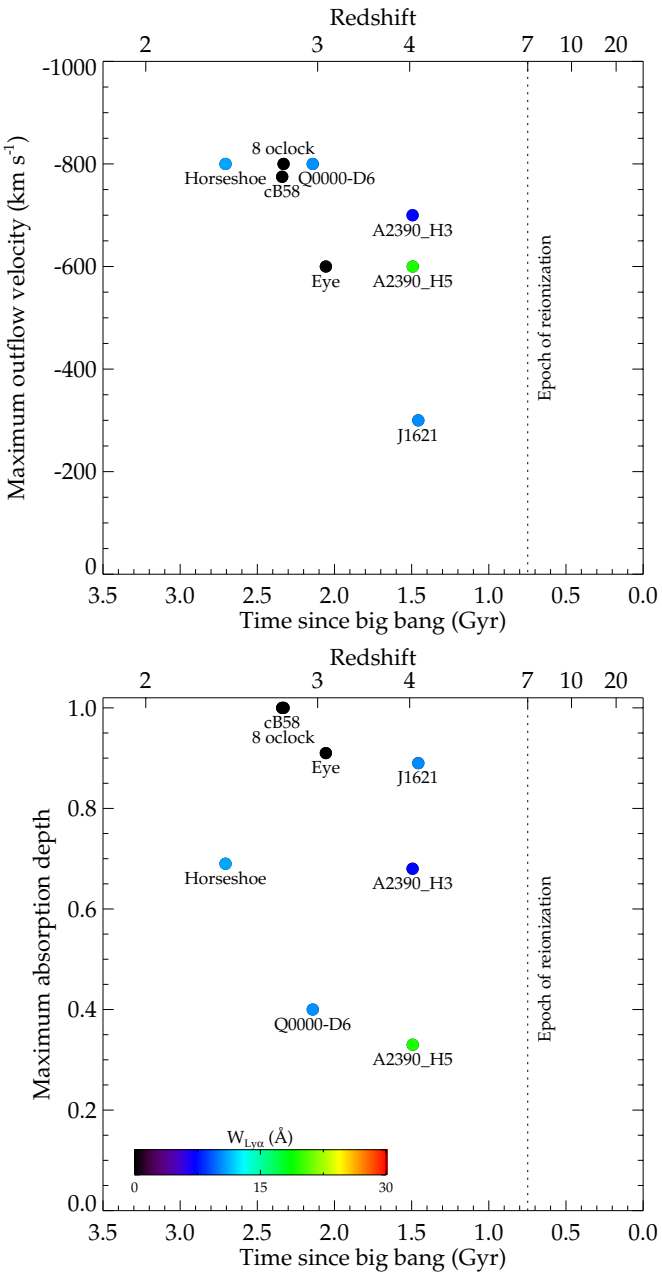

Figure 5. Outflow kinematics and covering fraction as a function of redshift. Top: maximum blueshifted velocity at which outflows are detected. In the case of A2390_H3 there is an uncertainty of ∼125 km s^{-1} arising from the unknown systemic redshift. Bottom: maximum depth of the average absorption profiles shown in Figure 3, which serves as a proxy for the covering fraction of H I at the corresponding velocity. We include estimated values for the 8 o'clock arc (Dessauges-Zavadsky et al. 2010) and a somewhat lower resolution ($R = 1300$) spectrum of Q0000-D6 (Steidel et al. 2010) in addition to the sources shown in Figure 3. Galaxies are color-coded according to their $W_{Ly\alpha}$, and relevant data are listed in Table 2. On average, the $z = 4$ galaxies show somewhat lower maximum outflow velocities and lower covering fractions (weaker absorption depth) compared to similarly studied sources at lower redshift, but the strongest trend is a decreasing covering fraction with $W_{Ly\alpha}$. The $z = 4$ data enable us to examine trends of H I covering fraction at a time significantly closer to the epoch of reionization, thought to end at $z \simeq 7$ (e.g., Schenker et al. 2012).

4.3. Trends with Lyα

We now turn to trends with Lyα equivalent width. Previous sections focused on possible redshift evolution of low-ionization absorption lines in our quest to examine whether this may signify an increasing ionizing escape fraction. The connection with Lyα is a natural one to explore given that there is a strong correlation between its equivalent width $W_{Ly\alpha}$ and low-ionization absorption (Jones et al. 2012; Shapley et al. 2003). Since our previous work has suggested that the distribution of $W_{Ly\alpha}$ for LBGs of a fixed luminosity increases with redshift (Stark et al. 2010, 2011; Schenker et al. 2012), we can hope to derive inferences about the low-ionization absorption in sources for which Lyα measurements are now widely available.

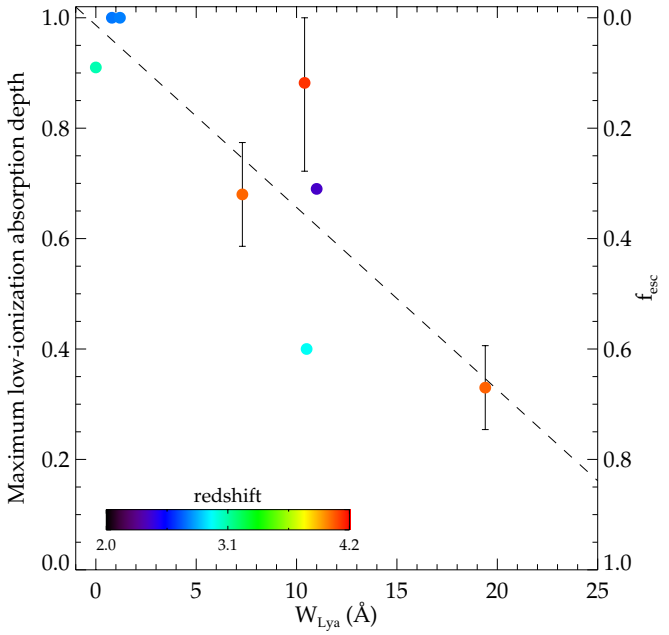

Figure 6. Correlation of Lyα equivalent width with H I covering fraction (and corresponding upper limit on f_{esc}) as traced by low-ionization absorption lines. The ordinate is identical to the lower panel of Figure 5, with 1σ uncertainties shown for the $z \simeq 4$ data. The dashed line is an unweighted linear fit to the data. Here $W_{Ly\alpha}$ includes only the emission component, and the two points at (1,1) are slightly offset for clarity. As discussed in the text, these absorption line measurements correspond to a lower limit on f_c and an upper limit on f_{esc}. Since Lyα emission strength increases with redshift (Stark et al. 2010, 2011), the anticorrelation of absorption line depth with $W_{Ly\alpha}$ likely indicates lower covering fractions (which would permit higher escape fractions) at earlier times.

Each galaxy in Figure 5 is color-coded according to $W_{Ly\alpha}$. This value refers only to the equivalent width of Lyα emission, differing from the conventional net sum of emission and absorption. The maximum outflow velocity is lower on average in galaxies with stronger Lyα emission, and although this trend is not statistically significant in our sample, it is consistent with well-quantified results from composite spectra (Shapley et al. 2003). More interestingly, Figure 5 reveals a trend of lower absorption depth (implying lower f_c) with stronger Lyα emission. The anticorrelation of absorption depth and $W_{Ly\alpha}$ has a Spearman rank coefficient $\rho = -0.81$ and is non-zero at a confidence level of 99.2%. We show this relation in Figure 6. In contrast, the trend of lower average f_c at higher redshift has limited significance ($\sim 1\sigma$) and is explained by Lyα demographics within the sample. Although limited by the small sample size, this is an important first quantitative result at these redshifts. Since the frequency and equivalent width of Lyα emission increase in LBGs at higher $z = 3 \rightarrow 6$, these results imply that the average covering fraction of low-ionization gas should decrease with redshift.

4.4. Ionizing Escape Fraction

Direct measurements of the ionizing flux are extremely difficult at the redshifts of interest in this paper because of

both the faint apparent magnitudes of LBGs and the high opacity of the Lyα forest. Nonetheless, we can provide important constraints on f_{esc} using indirect tracers of H I.

Before doing so, we consider the potential systematic uncertainties that may limit our ability to estimate the true value of f_{esc} from metal absorption lines. Results at $z \simeq 3$ have shown that f_{esc} is indeed dependent on low-ionization absorption strength (Bogosavljević 2010), although this relation is not one-to-one, likely due to the factors described below. While in general these preclude accurate estimates of the escape fraction, the maximum absorption depth (Figures 3 and 5) is a valuable constraint on H I spatial homogeneity and sets a stringent upper limit on f_{esc}.

1. We measure covering fraction as a function of velocity, yet gas at different velocities may cover different spatial regions, and we lack the spatial resolution needed to evaluate this effect. The maximum absorption depth *at a given velocity* is thus a lower limit on the total H I covering fraction and an upper limit on f_{esc}.
2. Metal-free H I is not detected. To date only two instances of metal-free gas have been found at these redshifts (Fumagalli et al. 2011), and so this is likely insignificant. Again, this possibility implies that covering fractions measured in Section 3 yield upper limits on f_{esc}.
3. Low column density gas will not be detected, although such gas will not affect f_{esc} unless it has very low metallicity $\lesssim$0.1 $Z_{\odot}$. The optical depth of metal transitions used here compared to Lyman continuum at ~900 Å is $(\tau/\tau_{LyC}) = 1.7$ for the weakest line (Si II λ1304) and 10–20 for the strongest transitions (Si II λ1260, C II λ1334, O I λ1302) for solar abundance ratios (Asplund et al. 2009). Galaxies in the $z = 2$–3 sample with measured interstellar abundance ratios have $Z \gtrsim 0.4\ Z_{\odot}$ for the relevant elements, such that the attenuation of weaker Si lines is roughly equal to that of ionizing radiation.
4. There may be narrow components with uniform covering fraction that are spectroscopically unresolved. However, such smooth absorption and column density profiles would require a remarkably regular spacing of discrete narrow components, and so a partial covering fraction appears more likely (see Pettini et al. 2002; Quider et al. 2009).
5. Si II and C II are present in both H I and H II regions. We have therefore confirmed that O I, with essentially the same ionization potential as H I, gives consistent results in all cases.
6. We measure a covering fraction at 1260–1526 Å, but the stars that are bright at these wavelengths do not necessarily emit at <912 Å. Our measurements therefore correspond to a constraint on the relative escape fraction $f_{esc,LyC}/f_{esc,1500}$ as commonly used in the literature. However, the spatial distribution of L_{1500} is similar to ionizing emission as traced by Balmer lines in $z \simeq$ 1–3 galaxies (e.g., Jones et al. 2010), indicating that this effect may be minimal.

With these caveats in mind, we now summarize what can be learned about the ionizing escape fraction at $z = 4$. The depth of low-ionization absorption lines gives upper limits $f_{esc} < 0.7$ for A2390_H5, <0.3 for A2390_H3, and <0.1 for J1621. The true values are likely well below the upper limits, and in three lower redshift galaxies we can verify that this is the case. Quider et al. (2010) show that the Cosmic Eye has an H I covering fraction of ≃95%, implying $f_{esc} < 0.05$ based on damped Lyα absorption, more stringent than the $f_{esc} < 0.1$ from our analysis. Second, no ionizing radiation is detected from the Horseshoe in deep UV imaging (B. Siana 2013, private communication) or from the spectrum of Q0000-D6 ($f_{esc} < 0.16$; Giallongo et al. 2002) despite low maximum covering fractions (Figures 3 and 5). Non-uniform coverage of low-ionization metals is evidently a necessary, but not sufficient, condition for the escape of ionizing radiation. Results derived in this paper should therefore be strictly interpreted as upper limits. Nonetheless, our measurements at $z = 4$ are readily compatible with derived photoionization rates in the IGM (e.g., Bolton et al. 2005; Faucher-Giguère et al. 2008), as well as a value $f_{esc} \gtrsim 0.2$ required for galaxies to reionize the universe at $z > 6$ (Robertson et al. 2013; Kuhlen & Faucher-Giguère 2012).

5. DISCUSSION

In our previous work (Jones et al. 2012) we found a decrease in the low-ionization absorption equivalent width with redshift in composite LBG spectra, but were unable to distinguish whether gas kinematics and/or covering fraction were the cause. The new data presented in this paper now resolve this ambiguity. The present data show an approximately equal decrease of ~25% in the gas velocity and covering fraction with redshift, although these differences are not statistically significant given the sample variance. A larger and well-defined sample would be needed to confirm such evolutionary trends. However, we also find a dependence (with 99.2% confidence) of low-ionization absorption depth with Lyα emission. This result suggests that the strong trend between Lyα and low-ionization absorption equivalent width (Jones et al. 2012; Shapley et al. 2003) is predominantly due to the covering fraction of neutral hydrogen.

The main limitation of methods used in this work to constrain f_{esc} is that we do not directly measure the fraction of ionizing emission covered by H I. While the spectrally resolved covering fraction of heavy elements provides an important measure of the "patchiness" of H I, gas at different velocities may cover different spatial regions, and so we can derive only a lower (upper) limit on f_c (f_{esc}). Deep integral field spectroscopy with good spatial resolution may resolve this issue and provide better constraints on f_c and f_{esc}.

We have successfully measured the kinematics and covering fraction of low-ionization (H I) gas in $z = 4$ LBGs from high-quality rest-UV spectra and investigated the implications for escaping ionizing radiation. Importantly, the new data enable these measurements at a time <1 Gyr from the reionization epoch, much earlier than was previously possible. In order for galaxies to reionize the universe, the ionizing escape fraction must increase rapidly from $\langle f_{esc} \rangle < 0.02$ at $z \sim 1$ (Siana et al. 2010) through $\langle f_{esc} \rangle \simeq 0.05$ measured at $z = 3$ (Bogosavljević 2010; Nestor et al. 2013) to a value $f_{esc} \gtrsim 0.2$ at $z = 7$ (Robertson et al. 2013; Kuhlen & Faucher-Giguère 2012). At $z = 4$ we derive an average maximum H I covering fraction $f_c = 0.63 \pm 0.16$, implying $\langle f_{esc} \rangle \lesssim 0.37$ for these sources. This value is readily consistent with an increasing escape fraction, as well as with requirements for reionization, although it is likely an overestimate of the true average f_{esc} for the reasons discussed in Section 4.4. Specifically for the $z \simeq$ 2–3 galaxies shown in Table 2, the derived average limit decreases from $\langle f_{esc} \rangle \lesssim 0.2$ from absorption line spectroscopy alone to $\lesssim$0.05–0.1 when combined with additional direct constraints on the Lyman continuum emissivity. The latter value is similar to the observed mean f_{esc} for LBGs at this redshift. At $z = 4$, IGM recombination rates suggest $f_{esc} \simeq$ 0.1–0.25 for star-forming galaxies (Bolton et al. 2005; Bolton & Haehnelt 2007;

Table 2
Spectroscopic Properties

ID	$W_{Ly\alpha}$ [a] (Å)	f_c [b]	v_{max} (km s^{-1})
Abell 2390_H3	7.3	0.68	700
Abell 2390_H5	19.4	0.33	600
SDSS J1621	10.4	0.89	300
cB58	~1	1.0	775
Cosmic Eye	~0	0.91	600
Horseshoe	11	0.69	800
8 o'clock arc	~1	~1.0	800
Q0000-D6	10.5	~0.4	800

Notes.
[a] Emission component only.
[b] Lower limit derived from absorption line depth.

Becker & Bolton 2013), which is also ~2–4 times below the limit we derive spectroscopically. Thus, although the f_{esc} limits we derive from spectrally resolved covering fractions may be overestimates, our results remain consistent with the increased ionizing emissivity over $2 < z < 5$ derived from IGM recombination rates (e.g., Becker & Bolton 2013) and the requirement that early galaxies dominated the reionization process.

While the trends with redshift are poorly constrained due to small samples, the available data reveal a reduced covering fraction with increasing $W_{Ly\alpha}$, indicating that galaxies with moderate or strong Lyα emission are likely to have larger f_{esc}. This is supported by direct evidence at $z = 3$, where high observed f_{esc} is correlated with stronger Lyα emission and weaker low-ionization absorption (Bogosavljević 2010; Nestor et al. 2013; Mostardi et al. 2013). Clearly the distribution of (metal-enriched) H I is patchier in galaxies with stronger Lyα emission, likely enabling a higher fraction of ionizing radiation to escape. Since the frequency and strength of Lyα emission in typical LBGs increase with redshift (Stark et al. 2010, 2011), our results provide new evidence that f_{esc} increases with redshift as a result of decreased H I covering fractions.

We thank Max Pettini for providing spectra of the $z = 2$–3 galaxies used as a comparison sample. We thank the anonymous referee for a detailed report that significantly improved the content and clarity of this paper. T.A.J. acknowledges support from the Southern California Center for Galaxy Evolution through a CGE Fellowship. D.P.S. acknowledges support from NASA through Hubble Fellowship grant HST-HF-51299.01 awarded by the Space Telescope Science Institute, which is operated by the Association of Universities for Research in Astronomy, Inc., for NASA under contract NAS5-265555. The analysis pipeline used to reduce the DEIMOS data was developed at UC Berkeley with support from NSF grant AST-0071048. This work relies on data obtained at the W. M. Keck Observatory, which is operated as a scientific partnership among the California Institute of Technology, the University of California, and the National Aeronautics and Space Administration, and was made possible by the generous financial support of the W. M. Keck Foundation. We wish to recognize the significant cultural role that the summit of Mauna Kea has within the indigenous Hawaiian community; we are most fortunate to have the opportunity to conduct observations from this mountain.

REFERENCES

Asplund, M., Grevesse, N., Sauval, A. J., & Scott, P. 2009, ARA&A, 47, 481
Bayliss, M. B., Hennawi, J. F., Gladders, M. D., et al. 2011, ApJS, 193, 8
Becker, G. D., & Bolton, J. S. 2013, arXiv:1307.2259
Bogosavljević, M. 2010, PhD thesis, California Institute of Technology
Bolton, J. S., & Haehnelt, M. G. 2007, MNRAS, 382, 325
Bolton, J. S., Haehnelt, M. G., Viel, M., & Springel, V. 2005, MNRAS, 357, 1178
Boutsia, K., Grazian, A., Giallongo, E., et al. 2011, ApJ, 736, 41
Conroy, C., & Kratter, K. M. 2012, ApJ, 755, 123
Dessauges-Zavadsky, M., D'Odorico, S., Schaerer, D., et al. 2010, A&A, 510, A26
Ellis, R. S., McLure, R. J., Dunlop, J. S., et al. 2013, ApJL, 763, L7
Erb, D. K., Pettini, M., Shapley, A. E., et al. 2010, ApJ, 719, 1168
Faucher-Giguère, C.-A., Lidz, A., Hernquist, L., & Zaldarriaga, M. 2008, ApJ, 688, 85
Fosbury, R. A. E., Villar-Martín, M., Humphrey, A., et al. 2003, ApJ, 596, 797
Frye, B., & Broadhurst, T. J. 1998, ApJL, 499, L115
Fumagalli, M., O'Meara, J. M., & Prochaska, J. X. 2011, Sci, 334, 1245
Giallongo, E., Cristiani, S., D'Odorico, S., & Fontana, A. 2002, ApJL, 568, L9
Heckman, T. M. 2002, in ASP Conf. Ser. 254, Extragalactic Gas at Low Redshift, ed. J. S. Mulchaey & J. Stocke (San Francisco, CA: ASP), 292
Heckman, T. M., Borthakur, S., Overzier, R., et al. 2011, ApJ, 730, 5
Hinshaw, G., Larson, D., Komatsu, E., et al. 2013, ApJS, 208, 19
Inoue, A. K., & Iwata, I. 2008, MNRAS, 387, 1681
Iwata, I., Inoue, A. K., Matsuda, Y., et al. 2009, ApJ, 692, 1287
Jones, T. A., Stark, D. P., & Ellis, R. S. 2012, ApJ, 751, 51
Jones, T. A., Swinbank, A. M., Ellis, R. S., Richard, J., & Stark, D. P. 2010, MNRAS, 404, 1247
Kuhlen, M., & Faucher-Giguère, C.-A. 2012, MNRAS, 423, 862
Leitet, E., Bergvall, N., Hayes, M., Linné, S., & Zackrisson, E. 2013, A&A, 553, A106
Martin, C. L., & Bouché, N. 2009, ApJ, 703, 1394
Mortlock, D. J., Warren, S. J., Venemans, B. P., et al. 2011, Natur, 474, 616
Mostardi, R. E., Shapley, A. E., Nestor, D. B., Steidel, C. C., & Reddy, N. A. 2013, arXiv:1306.1535
Nestor, D. B., Shapley, A. E., Kornei, K. A., Steidel, C. C., & Siana, B. 2013, ApJ, 765, 47
Oesch, P. A., Bouwens, R. J., Illingworth, G. D., et al. 2013, ApJ, 773, 75
Oke, J. B. 1974, ApJS, 27, 21
Paardekooper, J.-P., Khochfar, S., & Dalla, C. V. 2013, MNRAS, 429, L94
Pelló, R., Kneib, J. P., Le Borgne, J. F., et al. 1999, A&A, 346, 359
Pettini, M., Rix, S. A., Steidel, C. C., et al. 2002, ApJ, 569, 742
Quider, A. M., Pettini, M., Shapley, A. E., & Steidel, C. C. 2009, MNRAS, 398, 1263
Quider, A. M., Shapley, A. E., Pettini, M., Steidel, C. C., & Stark, D. P. 2010, MNRAS, 402, 1467
Razoumov, A. O., & Sommer-Larsen, J. 2010, ApJ, 710, 1239
Robertson, B. E., Furlanetto, S. R., Schneider, E., et al. 2013, ApJ, 768, 71
Sand, D. J., Treu, T., Ellis, R. S., & Smith, G. P. 2005, ApJ, 627, 32
Schenker, M. A., Stark, D. P., Ellis, R. S., et al. 2012, ApJ, 744, 179
Shapley, A. E., Steidel, C. C., Pettini, M., & Adelberger, K. L. 2003, ApJ, 588, 65
Siana, B., Teplitz, H. I., Ferguson, H. C., et al. 2010, ApJ, 723, 241
Stark, D. P., Ellis, R. S., Chiu, K., Ouchi, M., & Bunker, A. 2010, MNRAS, 408, 1628
Stark, D. P., Ellis, R. S., & Ouchi, M. 2011, ApJL, 728, L2
Steidel, C. C., Bogosavljević, M., Shapley, A. E., et al. 2011, ApJ, 736, 160
Steidel, C. C., Erb, D. K., Shapley, A. E., et al. 2010, ApJ, 717, 289
Yajima, H., Choi, J.-H., & Nagamine, K. 2011, MNRAS, 412, 411